J Appl Biotechnol Rep. 2024 September;11(3):1386-1395

Journal of
Applied Biotechnology Reports

doi 10.30491/jabr.2024.403269.1649

Original Article

# Comparing Binding Stability of Gamma Glutamyl Cysteine to NF-κB and p100 Using Molecular Dynamics Simulations and Free Energy Calculations with Implications for Anti-COVID-19 Drug Design

**Soheila Ghaderi [1], Shirin Tarahomjoo [1*]**

[1] Razi Vaccine and Serum Research Institute, Agricultural Research, Education and Extension Organization (AREEO), Karaj, Iran

**Corresponding Author:** Shirin Tarahomjoo, PhD, Assistant Professor, Razi Vaccine and Serum Research Institute, Agricultural Research, Education and Extension Organization (AREEO), Karaj, Iran. Tel: +98-263-4570038, E-mail: starahomjoo@gmail.com

**Received** June 25, 2023; **Accepted** January 21, 2024; **Online Published** September 20, 2024

**Abstract**

**Introduction:** Nuclear factor κB (NF- κB) contributes to inflammation and cytokine storm in COVID-19 patients. The NF- κB activity is inhibited by p100 protein binding and downregulated using glutathione. Gamma Glutamyl Cysteine (GGC) is also a glutathione precursor. In this study, we aim to compare GGC binding stability to p100 and NF-κB to elucidate its effectiveness in reducing NF-κB activity.

**Materials and Methods:** Tertiary structures were prepared by molecular graphics programs. Free binding energies of complexes were compared using molecular dynamics simulations and Auto Dock. Simulation outputs were analyzed using CMView.

**Results:** Analyzing RMSD values indicated quite stable binding of GGC to p100. Also, RMSD of the NF-κB-R complex was slightly lower than that of NF- κB at the simulation end. The Rg indicated less dense packing of p100 and its slight structural changes in the presence of GGC. Analyzing amino acid fluctuations using RMSF revealed an important role of Leu 450 and Phe 451 in interactions of p100 with GGC. Free binding energies of p100-GGC and NF-κB-GGC complexes were -6.972 kJ/mol and 25.857 kJ/mol respectively. These results showed that GGC attached stably to p100, whereas it did not bind to NF-κB. Contact maps of complexes and corresponding native structures were compared and slight structural changes were observed. The Interaction of P450 2C9 enzyme with GGC was more stable than that with Flurbiprophen.

**Conclusions:** According to the findings, we suggest an antiviral effect for GGC through its stable binding to p100 and enhancing p100 activity for NF-κB inhibition. These results are useful for drug design against COVID-19.

**Keywords:** COVID-19, Gamma Glutamyl Cysteine, Molecular Dynamics Simulation, Nuclear Factor κB, p100/IκBδ, Regulator

**Citation:** Ghaderi S, Tarahomjoo S. Comparing Binding Stability of Gamma Glutamyl Cysteine to NF-κB and p100 Using Molecular Dynamics Simulations and Free Energy Calculations with Implications for Anti-COVID-19 Drug Design. J Appl Biotechnol Rep. 2024;11(3):1386-1395. doi:10.30491/jabr.2024.403269.1649

## Introduction

Rapid treatment of COVID-19 patients showing symptoms of severe respiratory complications and acute respiratory distress syndrome (ARDS) is essential. The release of pro-inflammatory cytokines such as tumor necrosis factor-alpha (TNF-α), interleukin-1 beta (IL-1β), interleukin 6 (IL-6), and interleukin 8 (IL-8) have been observed in infectious disease including COVID-19.[1,2] These cytokines cause the adsorption of neutrophils to the lungs. The neutrophils are then activated and release toxic mediators resulting in the extensive production of free radicals and reactive oxygen.[3] The lung tissue was subjected to oxidative damage by these compounds.[4] The "cytokine storm", ARDS and fulminate myocarditis constitute the underlying pathophysiology of COVID-19 infections.[5] The nuclear factor-κB (NF-κB) activation was essential for the transcription of pro-inflammatory mediators genes associated with ARDS. Moreover, a critical role is played by NF-κB in the harmonization of multifaceted inflammatory reactions.[6,7]

The antioxidant therapy utilizing alpha lipoic acid, N-acetyl-cysteine and glutathione downregulated NF- κB and affected the NF- κB signaling.[8-12] Glutathione (GSH) is a tripeptide (L-c-glutamyl-L-cysteinyl-glycine), which protects cells against free radicals and electrophiles such as those form during inflammations.[13] It plays a crucial role in lung defense mechanisms, particularly in protecting the membrane integrity of the airspace epithelium. Therefore, glutathione prevents injury arising from free radicals and inflammations.[14] The important effect of the glutathione extracellular administration on the reduction of inflammations in lung diseases has been demonstrated in several studies.[15,16] Ahmed et al. demonstrated its role in neutralizing the effect of peroxynitrite-mediated DNA damage during acute inflammation by forming a stable glutathione-DNA adduct.[17] The endogenous glutathione deficiency could affect the

clinical manifestation of the COVID-19 disease through enhanced virus replications, oxidative damages of the lung, and hyper-inflammation.[18] A novel treatment against COVID-19 using a protocol including glutathione was suggested by Alamdari et al.[19]

The degradation of IκB inhibitors is essential to activate NF-κB transcription factors. The p100 protein, an IκB inhibitor of NF-kB, forms tetrameric complexes with NF-κB. The complex stability is increased through the NF-κB association and the assembly is critical for inhibition of NF-κB.[20] The NF-κB blocking is expected to circumvent "cytokine storm" and ADRS in COVID-19 pneumonia patients. Moreover, decreased inflammations were observed after blocking NF-κB and the cytokine formation by glutathione in a randomized controlled trial.[21] The tumor access to cysteine is increased using gamma-glutamyl transpeptidase (GGT) and as a result, the level of intracellular GSH is enhanced. Therefore, the tumors maintain their redox balance when facing reactive oxygen species (ROS) caused by prooxidant therapies against cancer and persist against the death imposed through oxidative stress.[22] COVID-19 patients under critical conditions showed enhanced levels of oxidative stress and damages in addition to low levels of glutathione.[23]

In this study, therefore, we assessed interactions of p100 and also NF-κB structures with Gamma Glutamyl Cysteine (GGC), the glutathione precursor, using molecular dynamics (MD) simulations (Figure 1). GGC was considered as the regulatory (R) ligand. We compared the stability of the R ligand-associated p100 structure with that of the R ligand-associated NF-κB structure using bioinformatics tools. The secondary and tertiary structures were analyzed in terms of structural elements and critical amino acids. A role for GGC in NF-κB inhibition was then suggested. These results are expected to apply to drug design against COVID-19.

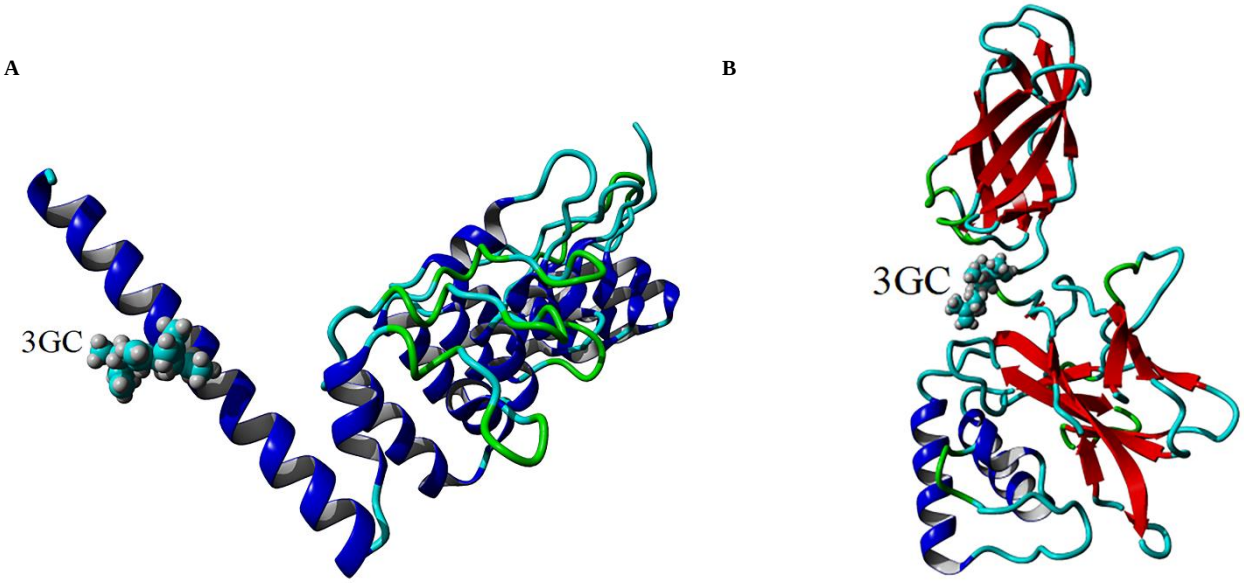


**Figure 1.** A) Snapshot of the p100-R complex after 50 ns simulation; B) Snapshot of the NF-κB-R complex after 50 ns simulation.

## Materials and Methods

The crystal structure of p100/NF-κB was obtained from the Protein Data Bank (PDB) under ID number 4ot9.[20] The crystal structure of NF-κB was retrieved from the PDB using ID number 1nfk.[24] The Deep View visualization was applied for previewing the files and replacing missing side chains with the added OXT at the C-terminus separately.[25] Three-dimensional structures were prepared using the molecular graphics program PYMOL, a robust, stable, and widely used program.[26] Auto Dock Tools were applied for all of the steps required for the setup and the analysis of docking runs.[27] Receptor-ligand docking was analyzed using Auto Dock Vina.[28] The ligand binding sites in NF-κB and p100 were chosen based on their crystalline structures. The ligand (3GC) was attached in the original PDB files including p100 and NF-κB structures as well as the docking protocol. In the Auto Dock Vina algorithm, the following parameters were set: (i) number of binding modes – 10, (ii) exhaustiveness of search – 8, and (iii) maximum energy difference - 3 kcal/mol. The pose with the maximum hydrogen bonds and the minimum change in the binding free energy, as shown in the View Dock window, was selected from all possible poses suggested by the Auto Dock Vina algorithm. These were further analyzed for hydrogen bond formations between functional groups of ligands and amino acids using the Biovia Discovery Studio (DS) visualizer.[29] Both proteins were prepared by removing heteroatoms, and adding hydrogens and charges. After identification of the binding site, we used GROMACS version 4.5.5 and Charmm36-jul2017.ff force field.[30] Then, we used the official CHARMM

General Force Field server (CGenFF server) to form complexes.[31] NF-κB-R and p100-R complexes were assessed using Yasara and Pymol viewers (32). Eventually, the topology and coordinate files were prepared with respect to the contents of the GROMACS system.[33] Simulations were done in pH 7 using periodic boundary conditions. The protonation fixing process was carried out at pH 7 using the H++ server, which served as input for molecular dynamics simulation.[34] Dimensions of the applied cubic boxes were 9.4, 7.4, and 7.6 $nm^3$ and the boxes were filled with appropriate numbers of water molecules. In order to neutralize the system, appropriate numbers of Na and Cl ions were added to the boxes. To eliminate any undesirable contact atoms and the initial kinetic energy in the simulation boxes, the energy was minimized by applying the steepest descent algorithm. Then each of the defined systems was equilibrated in two stages including NPT and NVT simulations for 5 ns at 310 K and 1 bar. The pressure and the temperature were controlled using Parrinello-Rahman barostat and V-rescale thermostat, respectively.[34-36] For each component of the systems, the PME algorithm was applied to estimate electrostatic interactions.[37] LINCS and SETTLE algorithms were used to fix chemical bonds in atoms of proteins and solvent molecules, respectively.[38-39] All of the simulations were run for 50 ns using the time step of 2fs. The MD simulations were done in two steps: (1) a 50 ns MD simulation was performed to optimize and refine 3D models of structures before docking, and (2) a second 50 ns MD simulation was done to examine the backbone stability of complexes including NF-κB-R and p100-R.[40] All of the simulations were repeated to test for the convergence of the results.

Average conformations of models were extracted from the trajectory and compared with the initial models using Yasara and Pymol softwares. These steps were repeated for each of the complexes and native structures. The binding free energy of each complex was calculated using the Molecular Mechanics Poisson-Boltzmann Surface Area (MM/PBSA).[41] ΔG estimates for the ligand association with proteins as the following:

$$\Delta G = G_{complex} - G_{protein} - G_{ligand} \quad (1)$$

The evaluation of equation (1) is done by two methods: (a) running separate trajectories of complex, protein, and ligand (b) evaluating all of the three terms of equation (1) using just snapshots from a trajectory on the complex. The method b is 2-3 times more efficient than the method a. However, method b assumes that free energies of snapshots of the protein and the ligand taken from the complex trajectory were comparable to those obtained from separate trajectories of the protein and the ligand. We have applied equation (1) using method b according to the study by Kuhn et al.[42]

Contact maps were created using the CM View software version 1.1.1.[43] When creating the contact maps, a distance cutoff of 8.0 Å was used for all of the atoms. Secondary and tertiary structures of proteins were obtained using the Yasara view software (www.yasara.org). The secondary structures of proteins and complexes were identified using Poly View server.[44]

The crystallography structure of the P450 2C9-Flurbiprophen complex was retrieved from Protein Data Bank (ID Number: Ir9o) and used to prepare the structure of P450 2C9- R ligand complex. The structure preparation and docking studies were carried out using Discover Studio Visualizer and AutoDock 4.2 respectively. PDBQT files of the ligand and the receptor were prepared using the AutoDock software. Then a.dpf and a. gpf files were provided for Grid and docking studies. The Docking process, complex interactions and energy calculations were performed using the Cygwin software. The interaction of the R- ligand with the P450 2C9 structure was then studied using the Yasara software.

## Results and Discussion

NF-κB is considered as a regulator of innate immunity.[45,46] It activates many pro-inflammatory cytokines, which contribute to increased inflammation and cytokine storms observed in COVID-19 patients.[47] IκB family members such as p100 carry out distinct cellular functions likely through their ability to inhibit NF-κB.[48-50]

To study interactions of the R-ligand with both p100 and NF-κB (Figure 1), we evaluated the stability of simulated trajectories by monitoring the root mean square deviation (RMSD) of the structures calculated using the primary experimental X-ray structures following GROMACS runs. RMSD of the complexes were compared with those of initial native structures. RMSD is a critical parameter to analyze the equilibration of MD trajectories. RMSD of the protein backbone atoms are plotted against time to check the stability of each system throughout the simulation.[51] The stability of the protein-ligand complex system was analyzed based on RMSD after 50 ns of MD simulations.[52] Profiles of RMSD for the NF-κB-R, p100-R, NF-κB, and p100 obtained from molecular dynamics simulations were shown in Figure 2. We compared RMSD of each complex with the corresponding native structure. RMSD values of p100 and p100-R were 0.36 nm and 0.31 nm respectively at the end of the simulations (Figure 2A). The RMSD value of NF-κB was 0.50 nm, and it reached to 0.48 nm for the NF-κB-R complex at the end of the simulation (Figure 2B). High deviations of RMSD values from initial native structures are attributed to the instability.[53] In this study, the RMSD value of the p100-R complex was slightly different from that of p100 at the end of the simulation indicating stability of the p100-R complex (Figure 2A). The RMSD value of the NF-κB-R

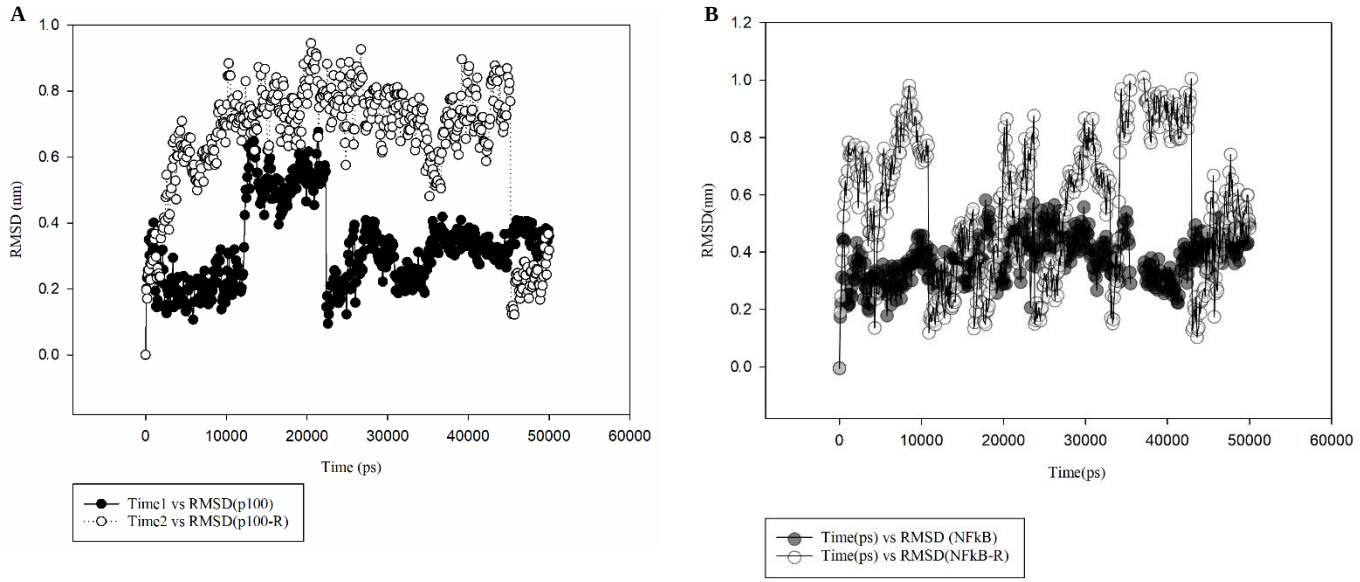


**Figure 2.** A) RMSD graph of p100 and p100 -R complex; B) RMSD graph of NF-κB and NFκB -R complex.

**Table 1.** Secondary Structures of p100-R, NFκB-R and the Corresponding Native Structures

| Secondary Structures (%) | p100-R | p100 | NF κB | NF-κB-R |
|---|---|---|---|---|
| Helix | 60.3 | 61.4 | 9.5 | 11.9 |
| Beta sheet | 0 | 1.1 | 36.5 | 35.6 |
| Turn | 13.5 | 9 | 10.4 | 10.3 |
| Coil | 26.2 | 28.5 | 43.6 | 42.3 |

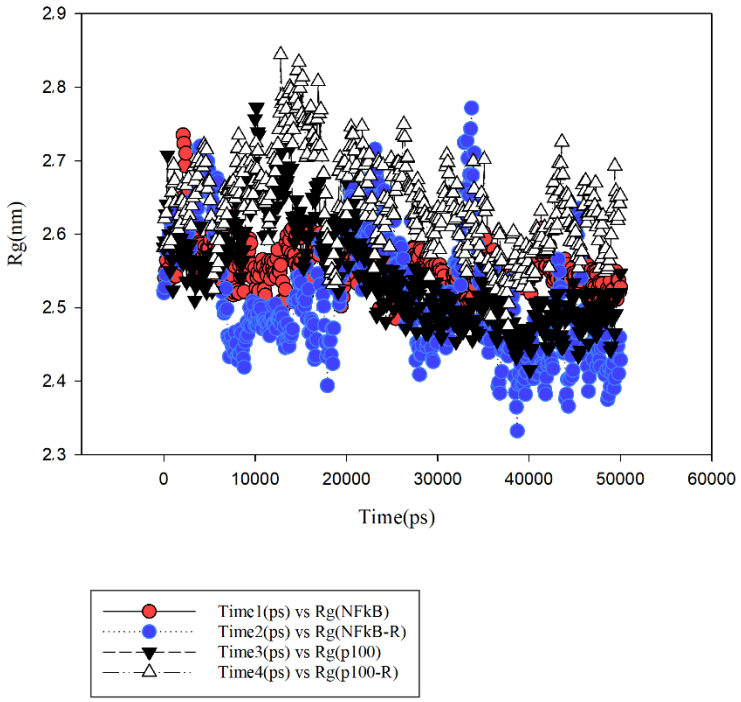


**Figure 3.** The Rg Graph of the p100-R and NFκB-R Complexes as Well as Native Structures.

complex was lower than that of the native structure, indicating the stability of NF-κB-R complex (Figure 2B). Comparing the secondary structure of p100-R with that of p100 revealed slight structural changes of p100 (Table 1). The secondary structure of NF-κB-R was also slightly different from that of NF-κB. Therefore, the R binding did not affect the stability of p100 and NF-κB significantly.

Radius of gyration (Rg) values of the NF-κB structure

and the NF-κB-R complex were 2.52 nm and 2.43 nm respectively (Figure 3). On the other hand, Rg values of the p100 protein and the p100-R complex were 2.54 nm and 2.65 nm respectively (Figure 3). The Rg value of the p100-R complex at 49000 ps, 49100 ps, 49400 ps, 49600 ps, and at 50000 ps (50 ns) were 2.601 nm, 2.633 nm, 2.69 nm, 2.65 nm, and 2.65 nm respectively. Therefore, Rg became stable at the end of the simulation. Also, Rg of the NF-κB-R complex was 2.4357 at 49500 ps and reached to 2.430 at 50 ns. These results indicated the conformational equilibrium of complexes and native structures. The protein stability is highly affected by the molecular packing. High packing densities have been observed in globular proteins, which are essential for maintaining the native structure of proteins and their stability.[54] The Rg gives information about the size and the compactness of proteins.[55] The overall chain size is indicated by the Rg as the basic measurement. The protein structural changes during MD simulations are quantified by Rg values. The Rg analysis for several proteins belonging to four major structural classes (α, β, α/β, and α+β) revealed that α-proteins possess the highest Rg values across the considered protein size range. Therefore, α-proteins packing densities were less than those of β- and (α+β) – proteins.[56] The dependence of the unfolded ensemble on denaturant concentration has been anticipated theoretically[57] and demonstrated in experiments and simulations.[58,59] Several correlations have been elucidated between the folding rate and the protein size. These correlations highlight the fact that folding rates decrease as protein size increases.[60,61] The Rg profile is able to describe not only the static compactness of a protein structure, but also the folding process from denatured state to native state.[62] Our results showed that Rg trends of two protein systems including p100 and NF-κB-R were downward, but NF-κB did not change significantly. The Rg of p100-R complex was slightly increased at the end of the simulations compared with the initial state. Therefore, the structural compactness of p100-R complex was not significantly different from that of its initial structure.

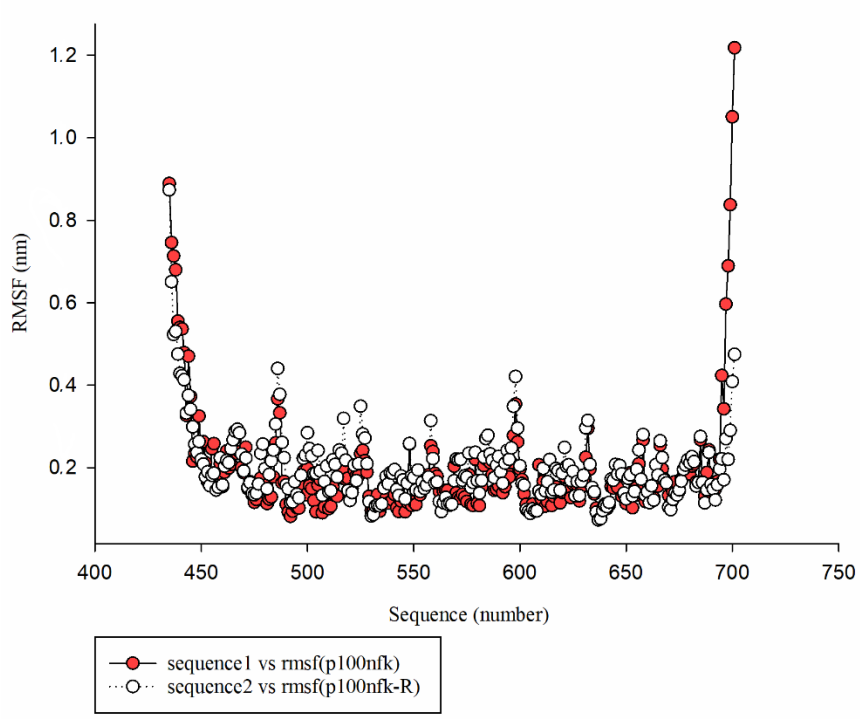


**Figure 4.** The RMSF Graph of p100-R and Native Structure.

The root mean square fluctuation (RMSF) is a measure of the average atomic mobility of backbone atoms (N, Cα, and C atoms), which are computed during MD simulations.[63] The amino acid fluctuations of p100 and its R complex were shown in Figure 4. The p100 protein and its R complex showed the highest amino acid fluctuations in the regions comprising of Gln435-Ala436 and Glu700-Pro701. These amino acids were located at the beginning and end of these structures (Figure 5A). The lower fluctuations and hence lower flexibilities were observed for Ala448-Gln455 residues (Figure 4). These key amino acids, which are involved in the interaction of p100 and R were depicted in Figure 5B. These results showed that two interactions were formed between Leu 450 and Phe 451 of p100 with R in the complex (Figure 5B). These interactions are expected to promote the R ligand affinity to p100.

Molecular mechanics energies in combination with Poisson-Boltzmann or generalized Born and surface continuum

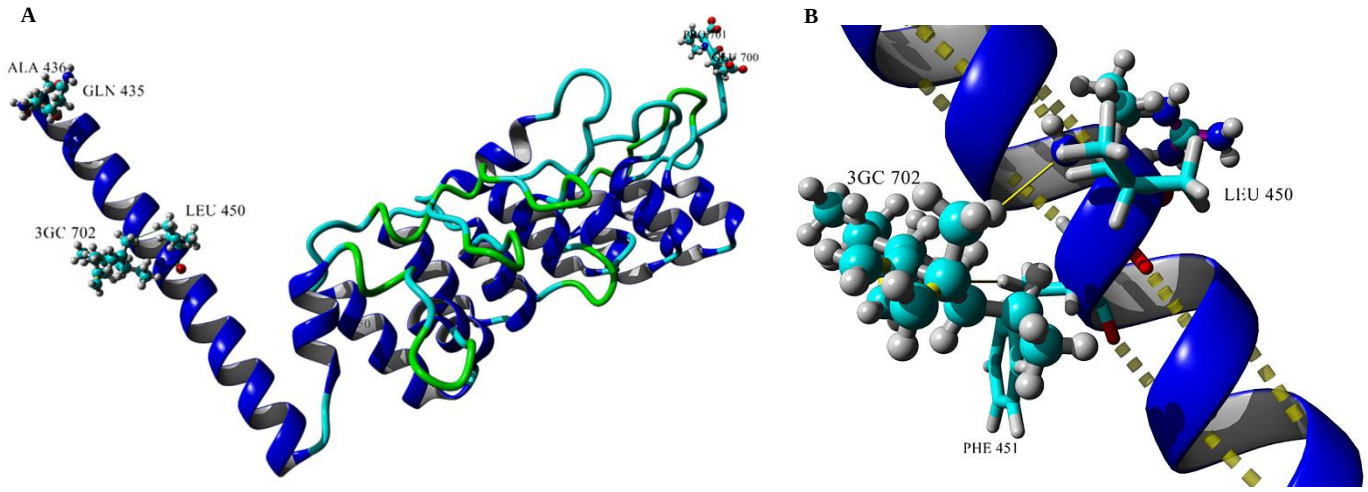


**Figure 5.** A) Snapshot showing highly fluctuating amino acids of the p100-R complex; B) Snapshot of the key amino acids involved in the interaction between p100 and R. The bold yellow line represents the interaction between Leu 450 and Phe 451 with R. Also, disconnected yellow line showed hydrogenic bonds in helix of p100.

**Table 2.** Gibbs Binding Energies of p100-R and NF-κB-R Complexes

| Gibbs Binding energies | p100-R (kJ/mol) | NF-κB-R (kJ/mol) |
|---|---|---|
| van der Waal energy | -18.406 +/- 4.065 | -0.046 +/- 0.028 |
| Electrostatic energy | -0.521 +/- 0.129 | -0.079 +/- 0.048 |
| Polar solvation energy | 14.704 +/- 5.487 | 25.939 +/- 10.895 |
| SASA energy | -2.712 +/- 0.565 | -0.074 +/- 0.254 |
| Binding energy (ΔG) | -6.972 +/- 6.772 | 25.857 +/- 10.976 |
| Protein solvation energy | -9870.640 | -13484.794 |
| 3GC solvation energy | -17.026 | -22.092 |
| Protein-3GC solvation energy | -9868.922 | -13449.733 |

solvation methods (MM/PBSA and MM/GBSA) have been proposed for estimating the binding free energy of biomacromolecules to small ligands. It's a common approach. They are usually based on molecular dynamics simulations of receptor-ligand complexes and therefore lie between empirical evaluations and strictly alchemical perturbation methods in terms of computational complexity and accuracy.[64] The Gibbs binding free energy of protein-ligand complexes is calculated by MM/PBSA method using a number of MD snapshots.[65,66] MM/PBSA algorithm is a valuable computational tool for analyzing bimolecular interactions. Simultaneous calculations of binding energy components and residue energy contributions by the MM/PBSA analysis tool are computationally less expensive. Free energy calculations based on molecular dynamics simulations show considerable promise for applications ranging from drug discovery to prediction of physical properties and structure-function studies.[67]

Multiple structures obtained from MD simulations are used to calculate Gibbs binding energy.[68-70] The binding of ligands to proteins happens if the change in Gibbs binding free energy (ΔG) is negative. Moreover, the ligand-protein association extent is determined by the negative ΔG magnitude. Therefore, it determines the binding affinity of a ligand to its acceptor.[71] The calculated binding energies (ΔG) of the p100-R and NF-κB-R complexes were -6.972 kJ/mol and 25.857 kJ/mol respectively (Table 2). The negative value of ΔG calculated for the p100-R complex demonstrated that the R ligand attached stably to p100. However, NF-κB did not bind to R regarding the positive ΔG value of the complex. Thus, the R ligand tends to bind p100 instead of NF-κB. Therefore, we suggest that the R antiviral effect was resulted from its stable binding to p100 and enhancing the p100 activity for the NF-κB inhibition.

We examined the structural differences of p100 and p100-R as well as those of NF-κB and NF-κB-R using contact maps (Figure 6). Protein contact maps are two dimensional representations of protein tertiary structures. These maps are used to compare the difference between protein structures.[72] The contact map of p100 was slightly different from that of p100-R at amino acids PRO 3, GLN 7, ALA 9, Glu 11, TYR 12, PHE 164, GLN 198, THR 202, ALA 233, GLY 234, and ASP 235 (Figure 6A). In addition, the contact map of NF-κB was marginally different from that of NF-κB-R at amino acids GLU 35, ASN 37, LYS 38, TYR 41, MET 215, LYS 285, ALA 287, ILE 283, ALA 287, LYS 305, and PRO 311 (Figure 6B). These results indicated that the tertiary structures of NF-κB and p100 were not affected significantly by the R ligand binding. Therefore, the R binding should not interfere with the p100 binding to NF-κB.

Docking studies were used to analyze the interaction of the R ligand with the cytochrome P450 2C9 enzyme. The

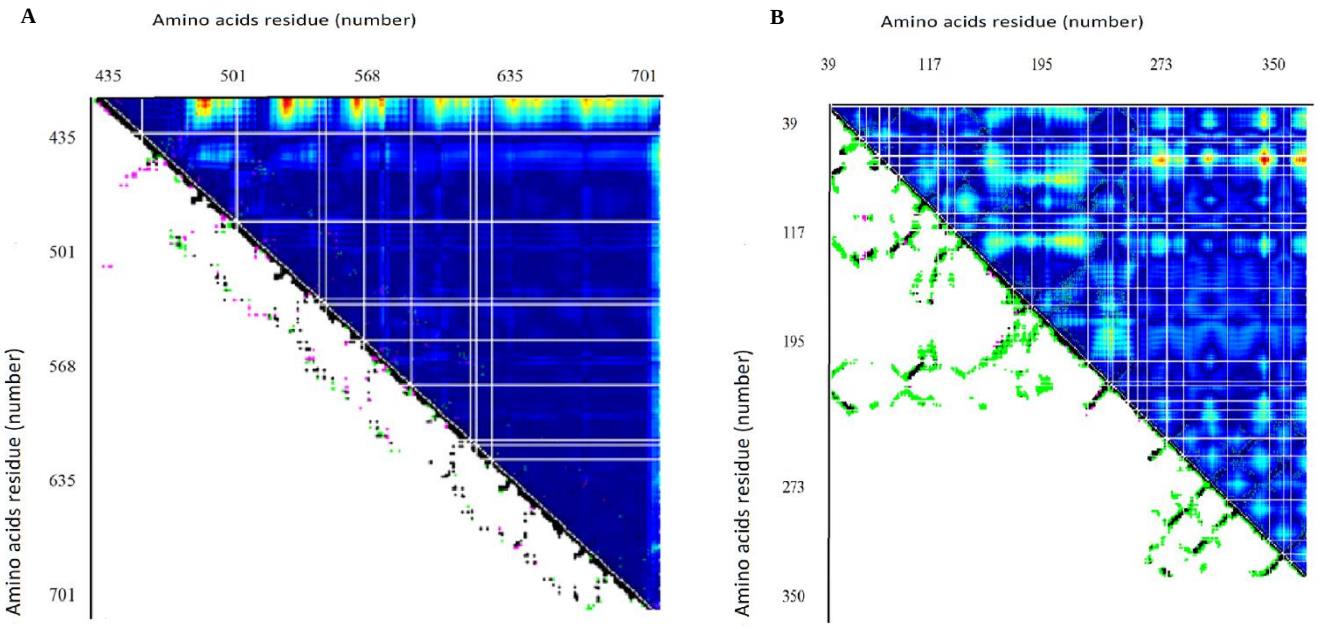


**Figure 6.** Comparing contact maps of complexes and initial native proteins. A) Comparing contact maps of the p100-R and its native structure; B) Comparing contact maps of the NF-κB-R and its native structure; Blue sections demonstrated the unchanged contacts between two structures, and red sections showed the contacts with the most difference between the two structures. Black dots showed the common contacts. The pink dots showed the contacts unique to the first structure and green dots were used for contacts unique to the second structure.

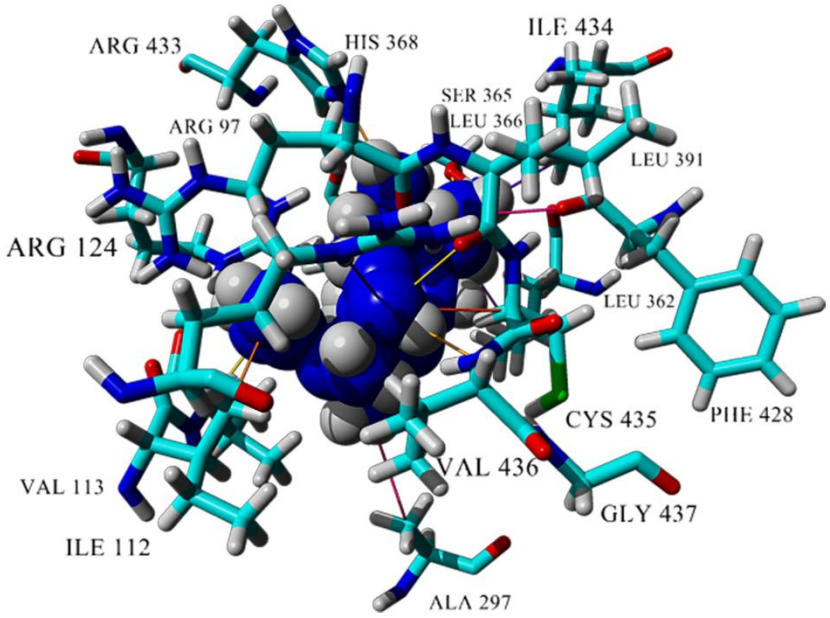


**Figure 7.** A Snapshot of the P450 2C9-R Complex. Amino acids involved in the interaction with the R-ligand were depicted.

**Table 3.** Comparing Energies and Properties of P450 2C9- Flurbiprophen and P450 2C9 – R Ligand

| Energy and properties | P450 2C9-flurbiprophen | P450 2C9- R ligand |
|---|---|---|
| Binding_energy(kJ/mol) | -7.68 | -8 |
| Vdw_energy | -6.75 | -6.24 |
| intermol_energy | -8.09 | -8.98 |
| Electrostatic_energy | -1.34 | -2.74 |
| Total _intermal | -0.14 | -1.49 |
| Torsional_energy | 0.55 | 2.47 |
| Ref_rms | 8.6 | 64.86 |
| Ligand efficiency | -0.43 | -0.5 |
| Inhibit_constant(uM) | 2.33 | 1.37 |

ligand showed interaction with P450 2C9 at amino acids Arg 124, Ala 297, Phe 428, Arg 433, Ile 434, Cys 435, Val 436, Gly 437, Leu 362, Ser 365, Leu 366, His 368, Leu 391, Arg 97, Val 113, and Ile 112 (Figure 7). Flurbiprofen was able to position itself in the active site cavity of P450 2C9.[73] Our docking results revealed that the interaction energy of P450 2C9-R ligand was lower than that of P450 2C9- Flurbiprofen (Table 3). Therefore, the interaction of P450 2C9-R ligand was more stable than that of P450 2C9- Flurbiprofen.

In this study, we used bioinformatics tools to assess the complexes in terms of the structure and the stability. Using these tools provides a fast and inexpensive method for the drug design studies. However, the obtained results need to be confirmed experimentally.

## Conclusion

Our results demonstrated that GGC stably binds to the p100 inhibitor of NF-κB. The GGC binding did not interfere with the p100 binding to NF-κB and enhanced the p100 inhibition activity. Also, the structural stability of the p100-R complex was confirmed using MD tools and free energy calculations. Moreover, GGC was able to interact with cytochrome P450. Therefore, a role for GGC in blocking NF-κB and hence controlling the COVID-19 inflammation is suggested. However, this role should be demonstrated experimentally. GGC is expected to be useful for drug design against COVID–19.

## Authors' Contributions

All the authors have contributed substantially to this work.

## Conflict of Interest Disclosures

The authors declare that they have no conflicts of interest.

## References


1. Martin TR. Lung cytokines and ARDS: Roger S. Mitchell lecture. Chest. 1999;116:2S-8S.
2. Wohlrab P, Kraft F, Tretter V, Ullrich R, Markstaller K, Klein KU. Recent advances in understanding acute respiratory distress syndrome. F1000Research. 2018;7. doi:10.12688/f1000research.11148.1
3. Windsor AC, Mullen PG, Fowler AA, Sugerman HJ. Role of the neutrophil in adult respiratory distress syndrome. Br J Surg. 1993;80(1):10-7. doi:10.1002/bjs.1800800106
4. Gadek JE, Pacht ER. The interdependence of lung antioxidants and antiprotease defense in ARDS. Chest. 1996;110(6):273S-7S. doi:10.1378/chest.110.6_Supplement.273S
5. Ruan Q, Yang K, Wang W, Jiang L, Song J. Clinical predictors of mortality due to COVID-19 based on an analysis of data of 150 patients from Wuhan, China. Intensive Care Med. 2020;46(5):846-8. doi:10.1007/s00134-020-05991-x
6. von Bismarck P, Klemm K, Wistädt CF, Winoto-Morbach S, Schütze S, Krause MF. Selective NF-κB inhibition, but not dexamethasone, decreases acute lung injury in a newborn piglet airway inflammation model. Pulm Pharmacol Ther. 2009;22(4):297-304. doi:10.1016/j.pupt.2009.02.002
7. Gasparini C, Feldmann M. NF-κB as a target for modulating inflammatory responses. Curr Pharm Des. 2012;18(35):5735-45. doi:10.2174/138161212803530763
8. Khachigian LM, Collins T, Fries JW. N-acetyl cysteine blocks mesangial VCAM-1 and NF-kappa B expression in vivo. Am J Pathol. 1997;151(5):1225-9.
9. Zhang WJ, FREI B. α-Lipoic acid inhibits TNF-a-induced NF-κB activation and adhesion molecule expression in human aortic endothelial cells. FASEB J. 2001;15(13):2423-32. doi:10.1096/fj.01-0260com
10. Suzuki YJ, Aggarwal BB, Packer L. α-Lipoic acid is a potent inhibitor of NF-κB activation in human T cells. Biochem Biophys Res Commun. 1992;189(3):1709-15. doi:10.1016/0006-291X(92)90275-P
11. Rahman A, Fazal F. Blocking NF-κB: an inflammatory issue. Proc Am Thorac Soc. 2011;8(6):497-503.
12. Cho S, Urata Y, Iida T, Goto S, Yamaguchi M, Sumikawa K, et al. Glutathione downregulates the phosphorylation of IκB: Autoloop regulation of the NF-κB-mediated expression of NF-κB subunits by TNF-α in mouse vascular endothelial cells. Biochem Biophys Res Commun. 1998;253(1):104-8. doi:10.1006/bbrc.1998.9697
13. Rahman I, MacNee W. Oxidative stress and regulation of glutathione in lung inflammation. Eur Respir J. 2000;16(3):534-54. doi:10.1034/j.1399-3003.2000.016003534.x
14. Li XY, Donaldson K, Rahman I, MacNee W. An investigation of the role of glutathione in increased epithelial permeability induced by cigarette smoke in vivo and in vitro. Am J Respir Crit Care Med. 1994;149(6):1518-25. doi:10.1164/ajrccm.149.6.8004308
15. Winterbourn CC. Revisiting the reactions of superoxide with glutathione and other thiols. Arch Biochem Biophys. 2016;595:68-71. doi:10.1016/j.abb.2015.11.028
16. Sedgeman CA, Su Y, Guengerich FP. Formation of S-[2-(N 6-Deoxyadenosinyl) ethyl] glutathione in DNA and Replication Past the Adduct by Translesion DNA Polymerases. Chem Res Toxicol. 2017;30(5):1188-96. doi:10.1021/acs.chemrestox.7b00022
17. Ahmed N, Chakrabarty A, Guengerich FP, Chowdhury G. Protective role of glutathione against peroxynitrite-mediated DNA damage during acute inflammation. Chem Res Toxicol. 2020;33(10):2668-74. doi:10.1021/acs.chemrestox.0c00299
18. Polonikov A. Endogenous deficiency of glutathione as the most likely cause of serious manifestations and death in COVID-19 patients. ACS Infect Dis. 2020;6(7):1558-62. doi:10.1021/acsinfecdis.0c00288
19. Alamdari DH, Moghaddam AB, Amini S, Alamdari AH, Damsaz M, Yarahmadi A. The application of a reduced dye used in orthopedics as a novel treatment against coronavirus (COVID-19): a suggested therapeutic protocol. Arch Bone Jt Surg. 2020;8(Suppl 1):291-4. doi:10.22038/abjs.2020.47745.2349
20. Tao Z, Fusco A, Huang DB, Gupta K, Young Kim D, Ware CF, et al. p100/IκBδ sequesters and inhibits NF-κB through kappaBsome formation. Proc Natl Acad Sci U S A. 2014;111(45):15946-51. doi:10.1073/pnas.1408552111
21. Yadav VS, Mishra KP, Singh DP, Mehrotra S, Singh VK. Immunomodulatory effects of curcumin. Immunopharmacol Immunotoxicol. 2005;27(3):485-97. doi:10.1080/08923970500242244
22. Hanigan MH. Gamma-glutamyl transpeptidase: redox regulation and drug resistance. Adv Cancer Res.

2014;122:103-41. doi:10.1016/B978-0-12-420117-0.00003-7
23. Kumar P, Osahon O, Vides DB, Hanania N, Minard CG, Sekhar RV. Severe glutathione deficiency, oxidative stress and oxidant damage in adults hospitalized with COVID-19: implications for GlyNAC (glycine and N-acetylcysteine) supplementation. Antioxidants. 2021;11(1):50. doi:10.3390/antiox11010050
24. Ghosh G, Duyne GV, Ghosh S, Sigler PB. Structure of NF-κB p50 homodimer bound to a κB site. Nature. 1995;373(6512):303-10. doi:10.1038/373303a0
25. Guex N, Peitsch MC. SWISS-MODEL and the Swiss-Pdb Viewer: an environment for comparative protein modeling. Electrophoresis. 1997;18(15):2714-23. doi:10.1002/elps.1150181505
26. Yuan S, Chan HS, Hu Z. Using PyMOL as a platform for computational drug design. Wiley Interdiscip Rev Comput Mol Sci. 2017;7(2):e1298. doi:10.1002/wcms.1298
27. Morris GM, Huey R, Lindstrom W, Sanner MF, Belew RK, Goodsell DS, et al. AutoDock4 and AutoDockTools4: Automated docking with selective receptor flexibility. J Comput Chem. 2009;30(16):2785-91. doi:10.1002/jcc.21256
28. Trott O, Olson AJ. AutoDock Vina: improving the speed and accuracy of docking with a new scoring function, efficient optimization, and multithreading. J Comput Chem. 2010;31(2):455-61. doi:10.1002/jcc.21334
29. Biovia DS. Materials Studio Modeling Environment. Dassault Systɯmes, San Diego. 2015.
30. Pezeshkian W, Khandelia H, Marsh D. Lipid configurations from molecular dynamics simulations. Biophys J. 2018;114(8):1895-907.
31. MacKerell Jr AD, Bashford D, Bellott ML, Dunbrack Jr RL, Evanseck JD, Field MJ, et al. All-atom empirical potential for molecular modeling and dynamics studies of proteins. J Phys Chem B. 1998;102(18):3586-616. doi:10.1021/jp973084f
32. Schrodinger LL. The PyMOL molecular graphics system. Version. 2015;1:8.
33. Terakawa T, Kameda T, Takada S. On easy implementation of a variant of the replica exchange with solute tempering in GROMACS. J Comput Chem. 2011;32(7):1228-34. doi:10.1002/jcc.21703
34. Anandakrishnan R, Aguilar B, Onufriev AV. H++ 3.0: automating p K prediction and the preparation of biomolecular structures for atomistic molecular modeling and simulations. Nucleic Acids Res. 2012;40(W1):W537-41. doi:10.1093/nar/gks375
35. Parrinello M, Rahman A, Vashishta P. Structural transitions in superionic conductors. Phys Rev Lett. 1983;50(14):1073. doi:10.1103/PhysRevLett.50.1073
36. Bussi G, Donadio D, Parrinello M. Canonical sampling through velocity rescaling. J Chem Phys. 2007;126(1). doi:10.1063/1.2408420
37. Darden T, York D, Pedersen L. Particle mesh Ewald: An N· log (N) method for Ewald sums in large systems. J Chem Phys. 1993;98(12):10089-92. doi:10.1063/1.464397
38. Hess B, Bekker H, Berendsen HJ, Fraaije JG. LINCS: a linear constraint solver for molecular simulations. J Comput Chem. 1997;18(12):1463-72. doi:10.1002/(SICI)1096-987X(199709)18:12<1463::AID-JCC4>3.0.CO;2-H
39. Miyamoto S, Kollman PA. Settle: An analytical version of the SHAKE and RATTLE algorithm for rigid water models. J Comput Chem. 1992;13(8):952-62. doi:10.1002/jcc.540130805
40. Rehman HM, Mirza MU, Ahmad MA, Saleem M, Froeyen M, Ahmad S, et al. A putative prophylactic solution for COVID-19: development of novel multiepitope vaccine candidate against SARS-COV-2 by comprehensive immunoinformatic and molecular modelling approach. Biology. 2020;9(9):296. doi:10.3390/biology9090296
41. Pearlman DA. Evaluating the molecular mechanics Poisson− Boltzmann surface area free energy method using a congeneric series of ligands to p38 MAP kinase. J Med Chem. 2005;48(24):7796-807. doi:10.1021/jm050306m
42. Kuhn B, Kollman PA. Binding of a diverse set of ligands to avidin and streptavidin: an accurate quantitative prediction of their relative affinities by a combination of molecular mechanics and continuum solvent models J Med Chem. 2000;43(20):3786-91. doi:10.1021/jm000241h
43. Vehlow C, Stehr H, Winkelmann M, Duarte JM, Petzold L, Dinse J, et al. CMView: interactive contact map visualization and analysis. Bioinformatics. 2011;27(11):1573-4. doi:10.1093/bioinformatics/btr163
44. Porollo AA, Adamczak R, Meller J. POLYVIEW: a flexible visualization tool for structural and functional annotations of proteins. Bioinformatics. 2004;20(15):2460-2. doi:10.1093/bioinformatics/bth248
45. Salminen A, Huuskonen J, Ojala J, Kauppinen A, Kaarniranta K, Suuronen T. Activation of innate immunity system during aging: NF-kB signaling is the molecular culprit of inflamm-aging. Ageing Res Rev. 2008;7(2):83-105. doi:10.1016/j.arr.2007.09.002
46. Baltimore D. Discovering NF-κB. Cold Spring Harb Perspect Biol. 2009;1(1):a000026.
47. Liu T, Zhang L, Joo D, Sun SC. NF-κB signaling in inflammation. Signal Transduct Target Ther. 2017;2(1):17023. doi:10.1038/sigtrans.2017.23
48. Sun SC, Ganchi PA, Beraud C, Ballard DW, Greene WC. Autoregulation of the NF-kappa B transactivator RelA (p65) by multiple cytoplasmic inhibitors containing ankyrin motifs. Proc Natl Acad Sci U S A. 1994;91(4):1346-50. doi:10.1073/pnas.91.4.1346
49. Tergaonkar V, Correa RG, Ikawa M, Verma IM. Distinct roles of IκB proteins in regulating constitutive NF-κB activity. Nat Cell Biol. 2005;7(9):921-3. doi:10.1038/ncb1296
50. O'Dea E, Hoffmann A. The regulatory logic of the NF-κB signaling system. Cold Spring Harb Perspect Biol. 2010;2(1):a000216. doi:10.1101/cshperspect.a000216
51. ul Qamar MT, Alqahtani SM, Alamri MA, Chen LL. Structural basis of SARS-CoV-2 3CLpro and anti-COVID-19 drug discovery from medicinal plants. J Pharm Anal. 2020;10(4):313-9. doi:10.1016/j.jpha.2020.03.009
52. Joshi T, Joshi T, Sharma P, Chandra S, Pande V. Molecular docking and molecular dynamics simulation approach to screen natural compounds for inhibition of *Xanthomonas oryzae* pv. Oryzae by targeting peptide deformylase. Journal of Biomolecular Structure and Dynamics. 2021;39(3):823-40. doi:10.1080/07391102.2020.1719200
53. Kumar A, Purohit R. Computational centrosomics: An approach to understand the dynamic behaviour of centrosome. Gene. 2012;511(1):125-6. doi:10.1016/j.gene.2012.09.040
54. Galzitskaya OV, Reifsnyder DC, Bogatyreva NS, Ivankov DN, Garbuzynskiy SO. More compact protein globules exhibit slower folding rates. Proteins: Struct Funct Bioinf. 2008;70(2):329-32. doi:10.1002/prot.21619
55. Arnittali M, Rissanou AN, Harmandaris V. Structure of biomolecules through molecular dynamics simulations. Procedia Comput Sci. 2019;156:69-78. doi:10.1016/j.procs.2019.08.181
56. Lobanov MY, Bogatyreva NS, Galzitskaya OV. Radius of

gyration as an indicator of protein structure compactness. Mol Biol. 2008;42:623-8. doi:10.1134/S0026893308040195
57. Alonso DO, Dill KA. Solvent denaturation and stabilization of globular proteins. Biochemistry. 1991;30(24):5974-85. doi:10.1021/bi00238a023
58. Schuler B, Lipman EA, Eaton WA. Probing the free-energy surface for protein folding with single-molecule fluorescence spectroscopy. Nature. 2002;419(6908):743-7. doi:10.1038/nature01060
59. Merchant KA, Best RB, Louis JM, Gopich IV, Eaton WA. Characterizing the unfolded states of proteins using single-molecule FRET spectroscopy and molecular simulations. Proc Natl Acad Sci U S A. 2007;104(5):1528-33. doi:10.1073/pnas.0607097104
60. Thirumalai D. From minimal models to real proteins: time scales for protein folding kinetics. J Phys I. 1995;5(11):1457-67. doi:10.1051/jp1:1995209
61. Koga N, Takada S. Roles of native topology and chain-length scaling in protein folding: a simulation study with a Gō-like model. J Mol Biol. 2001;313(1):171-80. doi:10.1006/jmbi.2001.5037
62. Hong L, Lei J. Scaling Law for Radius of Gyration and Its Dependence on Hydrophobicity. arXiv preprint arXiv: 0711.3679. 2007. doi:10.48550/arXiv.0711.3679
63. Vendome J, Posy S, Jin X, Bahna F, Ahlsen G, Shapiro L, et al. Molecular design principles underlying β-strand swapping in the adhesive dimerization of cadherins. Nat Struct Mol Biol. 2011;18(6):693-700. doi:10.1038/nsmb.2051
64. Genheden S, Ryde U. The MM/PBSA and MM/GBSA methods to estimate ligand-binding affinities. Expert Opin Drug Discov. 2015;10(5):449-61. doi:10.1517/17460441.2015.1032936
65. Baker NA, Sept D, Joseph S, Holst MJ, McCammon JA. Electrostatics of nanosystems: application to microtubules and the ribosome. Proc Natl Acad Sci U S A. 2001;98(18):10037-41. doi:10.1073/pnas.181342398
66. Kumari R, Kumar R, Open Source Drug Discovery Consortium, Lynn A. g_mmpbsa A GROMACS tool for high-throughput MM-PBSA calculations. J Chem Inf Model. 2014;54(7):1951-62. doi:10.1021/ci500020m
67. Klimovich PV, Shirts MR, Mobley DL. Guidelines for the analysis of free energy calculations. J Comput Aid Mol Des. 2015;29:397-411. doi:10.1007/s10822-015-9840-9
68. Karami M, Jalali C, Mirzaie S. Combined virtual screening, MMPBSA, molecular docking and dynamics studies against deadly anthrax: an in silico effort to inhibit Bacillus anthracis nucleoside hydrolase. J Theor Biol. 2017;420:180-9. doi:10.1016/j.jtbi.2017.03.010
69. Li CD, Xu Q, Gu RX, Qu J, Wei DQ. The dynamic binding of cholesterol to the multiple sites of C99: as revealed by coarse-grained and all-atom simulations. Phys Chem Chem Phys. 2017;19(5):3845-56. doi:10.1039/C6CP07873G
70. Liu C, Zhu Y, Tang M. Theoretical studies on binding modes of copper-based nucleases with DNA. J Mol Graph Model. 2016;64:11-29. doi:10.1016/j.jmgm.2015.12.003
71. Bronowska AK. Thermodynamics of ligand-protein interactions: implications for molecular design. Thermodynamics-Interaction Studies-Solids, Liquids and Gases: IntechOpen; 2011. doi:10.5772/19447
72. Emerson IA, Amala A. Protein contact maps: a binary depiction of protein 3D structures. Phys A: Stat Mech Appls. 2017;465:782-91. doi:10.1016/j.physa.2016.08.033
73. Wester MR, Yano JK, Schoch GA, Yang C, Griffin KJ, Stout CD, et al. The structure of human cytochrome P450 2C9 complexed with flurbiprofen at 2.0-E resolution. J Biol Chem. 2004;279(34):35630-7. doi:10.1074/jbc.M405427200